

Scalable interconnections for remote indirect exciton systems based on acoustic transport

S. Lazić,^{1,2,*} A. Violante,¹ K. Cohen,³ R. Hey,¹ R. Rapaport,³ and P. V. Santos¹

¹*Paul-Drude-Institut für Festkörperelektronik, Hausvogteiplatz 5-7, 10117 Berlin, Germany*

²*Departamento de Física de Materiales, Universidad Autónoma de Madrid, 28049 Madrid, Spain*

³*Racah Institute of Physics, The Hebrew University of Jerusalem, Jerusalem 91904, Israel*

(Received 17 March 2013; revised manuscript received 23 September 2013; published 26 February 2014)

Excitons, quasiparticles consisting of electron-hole pairs bound by the Coulomb interaction, are a potential medium for the processing of photonic information in the solid state. Information processing via excitons requires efficient techniques for the transport and manipulation of these uncharged particles. We have carried out a detailed investigation of the transport of excitons in GaAs quantum wells by surface acoustic waves. Based on these results, we introduce here a concept for the interconnection of multiple remote exciton systems based on the long-range transport of dipolar excitons by a network of configurable interconnects driven by acoustic wave beams. By combining this network with electrostatic gates, we demonstrate an integrated exciton multiplexer capable of interconnecting, gating, and routing exciton systems separated by millimeter distances. The multiplexer provides a scalable platform for the manipulation of exciton fluids with potential applications in information processing.

DOI: [10.1103/PhysRevB.89.085313](https://doi.org/10.1103/PhysRevB.89.085313)

PACS number(s): 71.35.-y, 73.21.Fg, 77.65.Dq, 78.55.-m

I. INTRODUCTION

The strong interaction with photons as well as with electronic excitations makes excitons ideal particles for the processing of photonic information. Within this approach, the information carried by photons is first converted to excitons, which are then manipulated by electric, optical, acoustic, or magnetic fields and subsequently reconverted to photons for further information transmission [1,2]. Exciton manipulation profits from strong nonlinearity in excitonic systems mediated by their electric-dipole interactions, which can be explored for the realization of all-optical control devices [3]. In addition, the interconversion between photons and excitons can be carried out coherently, i.e., by transferring the phase information between the two systems. The latter becomes especially interesting when combined with macroscopically coherent phases of either exciton polaritons [4,5] or indirect excitons (IX) [6,7], which provide a new platform for exciton-based information processing. Yet, the coherent manipulation of these excitonic phases as well as their integration into optoelectronic circuits remains a great challenge.

Excitons are metastable with lifetimes normally in the ns range for conventional direct excitons (DXs) and in the ps range for exciton polaritons. Applications require particles with long lifetimes, which can be efficiently stored, manipulated, and transported between different locations. Such a requirement is met by indirect excitons (IXs) in bilayer semiconductor systems consisting of two quantum wells (QWs) separated by a thin barrier, termed a double quantum well (DQW). As illustrated in the inset of Fig. 1(a), the application of a transverse electric field F_z forces the oppositely charged exciton constituents (i.e., electron and hole) into different QWs. The spatial charge separation enhances the IX radiative lifetime by orders of magnitude (up to a μ s range) as compared to DXs, while still maintaining the Coulomb correlation between the electrons and holes.

Different studies have addressed the manipulation of IXs on time scales shorter than their lifetime. The trapping of IXs

even down to the single-particle level [8] was demonstrated using a variety of potential landscapes created by optical [9], magnetic [10], electric [11,12], or strain [13] fields. Applied electric fields, in particular, can control the IX energy and lifetime via the quantum confined Stark effect (QCSE) induced by F_z [14]. Proposals for all-optical control via remote dipolar interactions of IX fluids have also been put forward [3]. Recently, Ref. [15] introduced an exciton optoelectronic transistor (EXOT), where the exciton flow (over a few tens μ m) induced by potential-energy gradients has been exploited for the realization of simple operations on photonic signals, such as directional switching and merging [16,17]. Several groups have also demonstrated the transport of IXs over longer distances by diffusion [18], drift [19], as well as by moving electrostatic lattices [20]. Finally, we have recently shown that IXs can be efficiently transported over several hundreds of μ m by the moving (and tunable) strain induced by a surface acoustic wave (SAW) propagating on the DQW structure [21]. In contrast to the conventional acoustic transport of electrons and holes by the piezoelectric field of a SAW [22], the IXs are transported by the strain-induced band-gap modulation created by a nonpiezoelectric SAW.

Previous reports have addressed the coupling of a reduced number of, in most cases, closely spaced IX systems. An interesting question is whether an approach can be envisaged to interconnect multiple remote IX sites separated by several hundreds of μ m, providing, therefore, a multifunctional and scalable technology for exciton-based optoelectronic circuits. In this paper, we first show that IXs can be efficiently manipulated and transported over long distances by SAW fields. By using an improved sample design, we demonstrate IX transport distances approaching 1 mm, which are a factor of 3 larger than in previous experiments [21]. We have also established that both exciton constituents (i.e., both electrons and holes) are carried along the DQW transport channel, whose lateral dimensions are determined by the width of the SAW beam. The very long transport distances are attributed to the stronger IX confinement by the band-gap modulation provided by SAWs with shorter wavelength and higher amplitudes. The effects of the stronger confinement are further addressed by

*lazic.snezana@uam.es

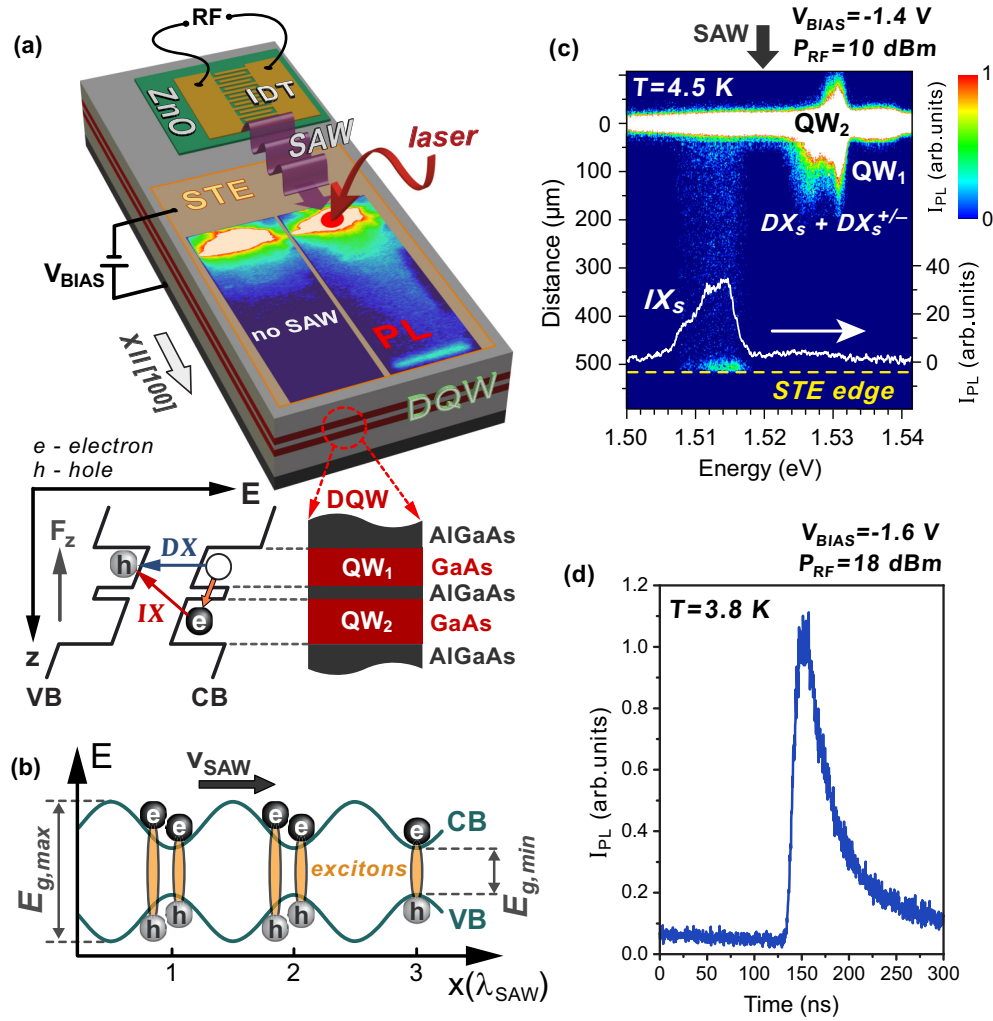


FIG. 1. (Color online) (a) Sample layout: Indirect excitons (IXs) photoexcited in the GaAs/(Al,Ga)As DQW are transported by a surface acoustic wave (SAW) launched by applying an electric power P_{RF} to an interdigital transducer (IDT) placed on a piezoelectric ZnO island. The SAW amplitude is stated in terms of the nominal RF power P_{RF} applied to the IDT. The IX lifetime and energy are controlled by the bias voltage V_{BIAS} applied between the semitransparent top electrode (STE) and the doped substrate. The superimposed PL images compare the emission in the absence and presence of a SAW. Inset: Energy-band diagram of a DQW along the growth (z) direction showing the direct exciton (DX) and indirect exciton (IX) transitions. (b) IX transport by the moving strain modulation of the conduction band (CB) and valence band (VB) in a DQW. $E_{g,min}$ ($E_{g,max}$) denotes minimum (maximum) band gaps induced by SAW strain field along the $x = [100]$ direction. (c) Spectral PL image of the transport channel at $T = 4.5$ K. The superimposed spectrum was recorded at the STE edge. (d) Time-resolved PL trace recorded at $T = 3.8$ K at the edge of the STE.

time-resolved investigations of the transport dynamics, which show that the IX are transported as well-defined packets moving with a velocity close to the acoustic velocity. We also demonstrate that IXs can be trapped and transported by moving IX dots created by the interference of two orthogonal SAW beams. These dots can transfer IXs from one to the other beam, thus providing a mechanism for the control of the propagation direction of the IX fluxes.

The previously mentioned features of the acoustic IX transport are combined to introduce a concept for the scalable interconnection of remote IX systems based on a network of acoustic beams and electrostatic gates. The feasibility of the concept is demonstrated by an exciton acoustic multiplexer (EXAM)—an integrated multiport device for the storage and controlled transfer of IXs between any two nodes of a two-dimensional (2D) array of IX systems. The EXAM

consists of a network of input/output (I/O) ports interconnected by an array of transport channels driven by SAWs. Each I/O port can be isolated from the array of transport channels by an exciton acoustic transistor (EXAT). As a result, these ports can be used for storage of IXs as well as for their interconversion to photons. Scalability, presently a main limitation for computational systems, is ensured by the sublinear dependence of the EXAM dimensions on the number of interconnected nodes. The experimental transport dynamics between the nodes is well-reproduced by a theoretical model of self-interacting IX fluids in a dynamic potential landscape, which successfully demonstrates the ability to design, simulate, and test complex IX devices. The EXAM concept is extensive and compatible with the well-established acoustic transport and manipulation of quantum excitations by SAWs [23–27].

In the following section (Sec. II), we describe the sample fabrication details as well as the optical techniques employed for the detection of IX transport and multiplexing. The experimental results are then presented in Sec. III. Here, we start with investigations of the dynamics of IXs under acoustic fields (Sec. III A), which demonstrate that SAW fields can capture IX packets and transport them over large distances. We then address the control of IX fluxes, which is carried out using EXATs (Sec. III B). In Sec. III C, the flow control by EXATs is then combined with long-range acoustic transport to realize an IX multiplexer. Finally, Sec. IV discusses issues regarding the application of EXAMs as a building block for integrated optoelectronic devices based on IXs and summarizes the main conclusions of this work.

II. EXPERIMENTAL DETAILS

The experiments were carried out on an (Al,Ga)As field-effect heterostructure containing three sets of DQWs grown on a n^+ -doped GaAs (001) wafer by molecular-beam epitaxy. Each DQW consists of two GaAs QWs with thickness of 14 and 17 nm [QW₁ and QW₂, respectively—cf. lower right inset in Fig. 1(a)] separated by a 4-nm-thick Al_{0.33}Ga_{0.67}As tunneling barrier. The DQWs were positioned at a depth of 700 nm below the sample surface within an undoped 2.5- μm -thick GaAs/(Al,Ga)As superlattice (SL).

The electric field F_z is induced by a reverse bias V_{BIAS} applied across the Schottky diode formed between a 10-nm-thick semitransparent titanium electrode (STE) on the sample surface and the n^+ -doped substrate, which serves as the common ground [cf. Fig. 1(a)]. The lower left inset shows the bending of the conduction band (CB) and valence band (VB) edges along the growth (z) direction induced by F_z . The excitons are locally excited underneath the STE area by a 780 nm pulsed diode laser (average power density of approximately 12 J/cm²). The use of SLs reduces the leakage photocurrents to values below 1 nA (for bias between -2 and 2 V and laser excitation power in the range up to a few tens of μW), thus ensuring that IXs are only formed by photoexcited carriers.

The Rayleigh SAWs (with wavelength $\lambda_{\text{SAW}} = 2.8 \mu\text{m}$ corresponding to a SAW frequency $f_{\text{SAW}} = 1 \text{ GHz}$ at helium temperatures) were electrically excited along a (100) surface direction by applying a radio-frequency (RF) signal to interdigital transducers (IDTs) deposited on piezoelectric ZnO islands. These SAWs do not carry a piezoelectric field outside the IDT region, thus preventing field-induced exciton dissociation [21]. Their strain field creates, via the deformation potential interaction, the moving type-I modulation of the CB and VB edges of the DQW [28] displayed in Fig. 1(b). Here, $E_{g,\text{min}}$ ($E_{g,\text{max}}$) denotes the minimum (maximum) band gap at the SAW phases of largest tensile (compressive) strain. Photoexcited IXs are captured close to the regions of $E_{g,\text{min}}$, which move with the acoustic velocity v_{SAW} [21]. The confinement of the electron and the hole at the same lateral (i.e., along the surface) coordinate prevents exciton dissociation, thus making this approach qualitatively different from charge transport by the type-II band-gap modulation induced by the piezoelectric SAWs. The depth of the DQW structures was selected in order to obtain a type-I potential

with approximately equal modulation amplitudes for the conduction and valence bands [21].

The transport of IXs by the SAW strain field is tracked by imaging the photoluminescence (PL) emitted via exciton recombination along the SAW transport path. The laser excitation was focused onto a 5 μm (10 μm) spot on the top semitransparent electrode by a 10 \times (5 \times) microscope objective. The light emitted along the SAW transport channel was collected by the same objective, dispersed by a single grating spectrometer, and imaged onto a cooled charge coupled device (CCD) camera with spatial resolution of 1 μm (2 μm).

III. RESULTS

A. Acoustic exciton transport

The two PL images superimposed on the device structure of Fig. 1(a) compare the excitonic PL in the absence (left plot) and presence (right plot) of a SAW. While in the former the emission is restricted to the region near the excitation spot, the latter shows substantial PL at the edge of the STE located approximately 500 μm away from the laser spot. The remote PL is attributed to the recombination of IXs transported by the SAW at the edges of the STE, where the sudden reduction of the vertical field F_z creates a potential barrier blocking the IX transport [12]. As the IXs are pushed by the SAW against this barrier, their concentration increases while the lifetime reduces, thus resulting in a stronger PL.

The long-range transport of IXs is confirmed by the spectral dependence of the PL along the transport channel displayed in Fig. 1(c). The PL around 1.53 eV is dominated by the recombination of spatially direct neutral exciton (DX) and charged exciton (DX[±]) complexes associated with the two QWs. This emission extends to distances of up to approximately 150 μm from the generation point due to the expansion of hot excitons and free carriers created by the pulsed laser [29,30]. In contrast, the remote emission near the STE edge only shows the redshifted PL signal, which is attributed to the recombination of acoustically transported IX packets. The energy of this remote PL is determined (via the QCSE) by the bias applied to the STE. The PL intensities integrated over the transport channel with and without a SAW differ by less than 1%, demonstrating that the SAW transports the excitons, introducing negligible losses. The exciton transport efficiency of about 50% over a distance of 500 μm was estimated calculating the ratio between the integrated PL intensity for IXs at the excitation point in the absence of SAW and at the recombination point for $P_{\text{RF}} = 10 \text{ dBm}$ [cf. Fig. 1(c)].

The dynamics of the IX transport was probed by time-resolved PL measurements at the end of the SAW transport channel, as illustrated in Fig. 1(d). From the delay of the PL pulse onset, we calculate a maximum propagation velocity of $2.4 \pm 0.1 \mu\text{m/ns}$, which is close to the SAW group velocity of $v_{\text{SAW}} = 2.6 \pm 0.1 \mu\text{m/ns}$. The width of the PL pulse is determined by the initial size of the IX cloud created by the pulsed laser excitation. We observe a slight broadening of the PL profile as well as the development of a tail with increasing transport distances. These features, which are addressed in detail elsewhere [31], are attributed to trapping sites along the transport path induced by potential fluctuations, which capture

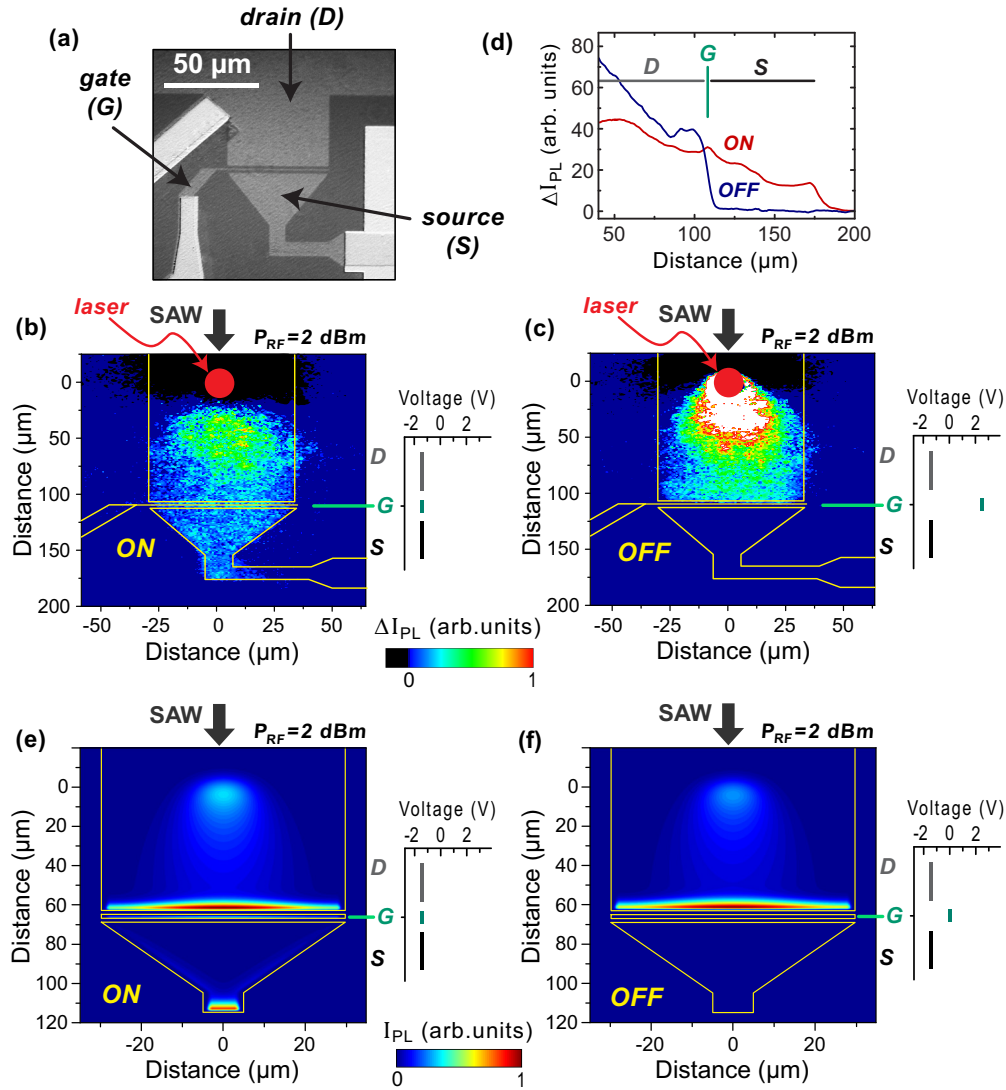


FIG. 2. (Color online) (a) Top view of the EXAT showing the source (S), drain (D), and gate (G) electrodes. The G electrode is $1.5 \mu\text{m}$ wide and separated by the same distance from the adjacent S and D regions. The lower color plots display PL images of the acoustic transport of IXs across the EXAT recorded in the (b) ON state (with biases $V_S = V_D = V_G = -1.4 \text{ V}$; cf. right inset) and (c) OFF state ($V_S = V_D = -1.4 \text{ V}$, $V_G = 2.5 \text{ V}$; cf. left inset). In both cases, the IXs were driven by a SAW generated using $P_{\text{RF}} = 2 \text{ dBm}$. The filled circles mark the position of the laser excitation spot. (d) Spatially resolved ΔI_{PL} profiles along the transport channel in the ON (red curve) and OFF (blue curve) states. (e),(f) The corresponding time-averaged PL profiles calculated by a numerical model (see text). The overlays indicate the positions of the drain, gate, and source electrodes.

IX and delay their propagation. The transport within well-defined μm -sized packets over long distances and at constant velocity contrasts with conventional diffusion [18] or drift-driven [15–17,19,20] processes, where the IX fluid undergoes self-expansion. In addition, it enables synchronization with pulsed optical excitation by appropriately selecting the SAW frequency.

Finally, it is interesting to compare the characteristics of the acoustic transport with the IX drift process in a potential gradient reported in Ref. [19]. IXs in a potential gradient induced by an electrostatic energy difference ΔE over the channel length L will drift with a velocity $v_{\text{IX}} = \mu_{\text{IX}} \Delta E / (eL)$. Here, μ_{IX} is the exciton mobility and e is the electron charge. Note that in this approximation, the transport velocity becomes inversely proportional to the channel length. If we assume

$\Delta E = 20 \text{ meV}$ [11] and use $\mu_{\text{IX}} = 2.3 \times 10^4 \text{ cm}^2/(\text{Vs})$ (from Ref. [21]), then v_{IX} becomes smaller than the SAW velocity already for very short transport lengths ($L > 16 \mu\text{m}$). Furthermore, the transport over the $L = 500 \mu\text{m}$ distance in Fig. 2 at the SAW speed would require (under the same assumptions) an unrealistically large ΔE of 650 meV . The limited range of ΔE also reduces the transport efficiency. In contrast, the qualitatively different nature of the acoustic transport enables one to transport well-defined IX packets over long distances with a well-defined velocity [cf. Fig. 1(d)].

B. Acoustic exciton transistor—EXAT

The SAW-driven long-range IX flow can be efficiently controlled by an acoustic exciton transistor (EXAT) placed

on the transport path. The EXAT electrode configuration [cf. Fig. 2(a)] is similar to the exciton optoelectronic transistor introduced in Refs. [15–17]. Here, the voltage applied to the gate electrode (G) creates (via the QCSE) a tunable energy barrier, which controls the acoustically driven IX flow between the source (S) and the drain (D) electrodes. In contrast to its optoelectronic counterpart, the IX flow through the EXAT is acoustically (rather than diffusion or drift) driven, with the flow direction defined by the SAW propagation direction. Note that in an EXAT, the roles of the source and drain electrodes are interchangeable simply by reversing the SAW propagation direction (not shown). To simplify the notation, we denote by *source* the port with the smaller area.

The switching action of the EXAT is demonstrated by the differential PL (ΔI_{PL}) images in Figs. 2(b) and 2(c). These images display the changes induced by the SAW and were obtained by subtracting PL images recorded in the presence and absence of the acoustic excitation. In both cases, excitons were optically excited on D, which was kept at the same bias voltage as S ($V_S = V_D = -1.4$ V). Note that the negative ΔI_{PL} values around the excitation spot are due to the IX extraction by the SAW and their transport along the SAW propagation direction. In the ON state [Fig. 2(b)], IXs can be easily transferred from D to S by applying a gate voltage, $V_G = V_S = V_D$ [cf. right inset of Fig. 2(b)]. The fringe electric field at the edges of the electrodes induces a potential barrier for IXs between S and G and between G and D, even when all electrodes are at the same potential. This barrier, however, is low in the ON state and can be easily surmounted by the

acoustic field. The transport, however, becomes completely blocked when the gate voltage is increased to $V_G = 2.5$ V [OFF state in Fig. 2(c)]. The switching efficiency is quantified in Fig. 2(d), which compares ΔI_{PL} profiles along the SAW transport channel in the OFF and ON states. While the purely electrostatic EXOT of Refs. [15–17] requires an electrostatic potential gradient between source and drain [32], the EXAT can be operated with these two ports at the same bias levels.

Figures 2(e) and 2(f) compare the experimental results for the IX transport across an EXAT [Figs. 2(b) and 2(c)] with a numerical modeling of the dynamics of the IX fluid [Figs. 2(e) and 2(f)]. This model, which uses the experimental sample parameters, includes the mutual interactions between IXs and the external potential induced by the electrostatic gates and the SAW. Details of the model together with additional simulation results (including videos demonstrating the EXAT operation) are contained in the Supplemental Material (SM) [33]. The numerical analysis of the IX transport across the EXAT described in the SM shows that the effect of the source, gate, and drain edges on the exciton flow is negligible when the EXAT is in the ON state. The good agreement between the experiment and modeling confirms that the device functions are well predicted by our model of IX fluid dynamics in mobile potentials.

The electrically controlled separation between the input and output ports (i.e., S and D electrodes) in the EXAT allows us to prove that the acoustic field really transports both exciton constituents (i.e., both electrons and holes) along the DQW

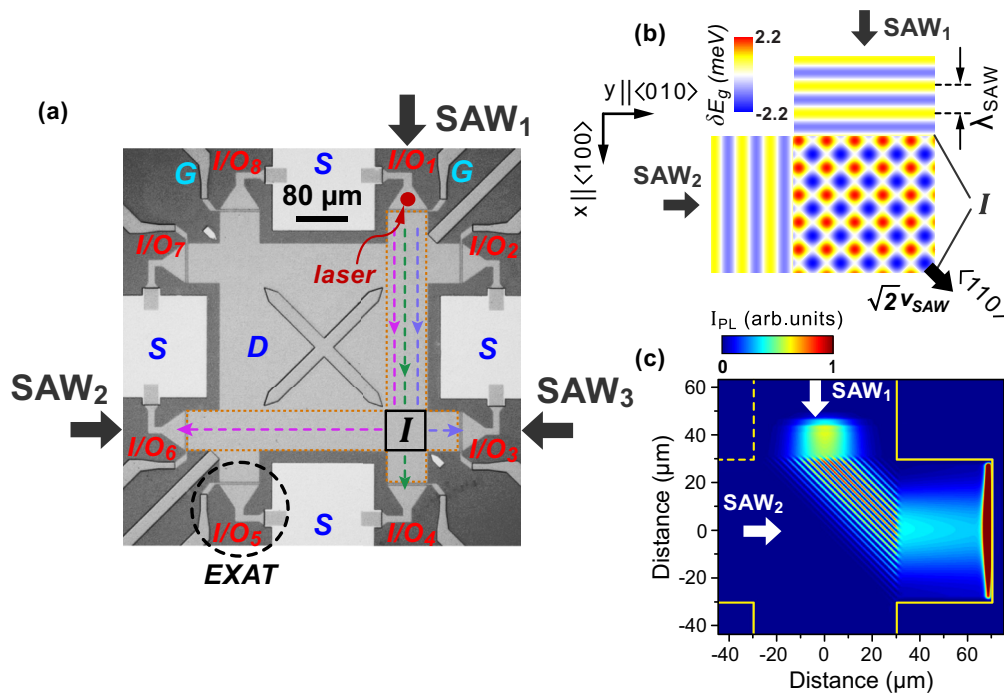


FIG. 3. (Color online) (a) Top view of the acoustic exciton multiplexer (EXAM): each I/O area contains an exciton optoelectronic transistor (EXAT) and an IDT for SAW generation (not shown). The vertical (horizontal) dotted rectangle delineates the transport channel formed by SAW₁ (SAW₂ or SAW₃) underneath the common drain. The dashed arrows indicate IX transfer between SAW₁, SAW₂, and SAW₃. The solid square labeled *I* denotes the intersection region of SAW₁ and SAW₂ (or SAW₁ and SAW₃). (b) Array of moving potential dots formed by SAW interference at *I*. (c) Simulated time-averaged emission pattern within *I* showing the IX transfer between SAW₁ and SAW₂.

structure. This question is relevant since the remote PL in IX transport experiments under a single STE can also be induced by the recombination of one type of carrier transported along the semiconductor channel with carriers of opposite polarity injected from the contacts (as for the IX bright spots reported in Ref. [7]).

In order to address this issue, we have determined the absolute sensitivity of the setup, which is defined as the photon flux required for a given count rate measured on the CCD camera detecting the PL. The sensitivity calibration was carried out using a reference laser beam reflected on a metal film deposited on the sample surface. Knowing the reflectance of the metal, it is possible to estimate the absolute reflected flux of photons. The ratio between the photon flux collected by the microscope objective in front of the sample and the CCD count rate gives the required calibration coefficient. The number of photons generated via the recombination of IXs was determined from the measured CCD count rate by taking into account the collection angle (which depends on the refractive index of the sample layers and on the numerical aperture of the objective lens) and the transmission of the semitransparent metal electrodes. If the PL signal comes from the recombination of one type of carrier transported by the SAW with carriers of opposite polarity electrically injected

from the electric contacts, we expect the contact current to be given by $I_c = eN_{\text{ph}}$, where N_{ph} is the detected photon flux and e is the electron charge. If the measured current is much less than I_c , then most of the electrons or holes forming the IXs must have been transported along the DQW structure by the SAW. For the experimental conditions of Fig. 2(b), where the laser beam is placed on the drain electrode, the measured photon flux in the source of the EXAT would require a source current, $I_c \approx 50$ nA. This current is two orders of magnitude larger than the measured source current (of 0.5 nA) under the same illumination conditions, showing that both electrons and holes must have been transported along the DQW channel by the SAW. Similar results were obtained for the current in the drain electrode, where recombination takes place at the edge of the drain area.

C. Acoustic exciton multiplexer—EXAM

We now introduce the EXAM [cf. micrograph of Fig. 3(a)], a device capable of routing IX fluids between different input/output ports (I/O_i , labeled by the port index $i = 1, \dots, 8$). Each I/O port contains an IDT (not shown) to generate an outgoing SAW beam as well as an exciton acoustic transistor [EXAT; cf. Fig. 2(a)] to control the IX flux between the

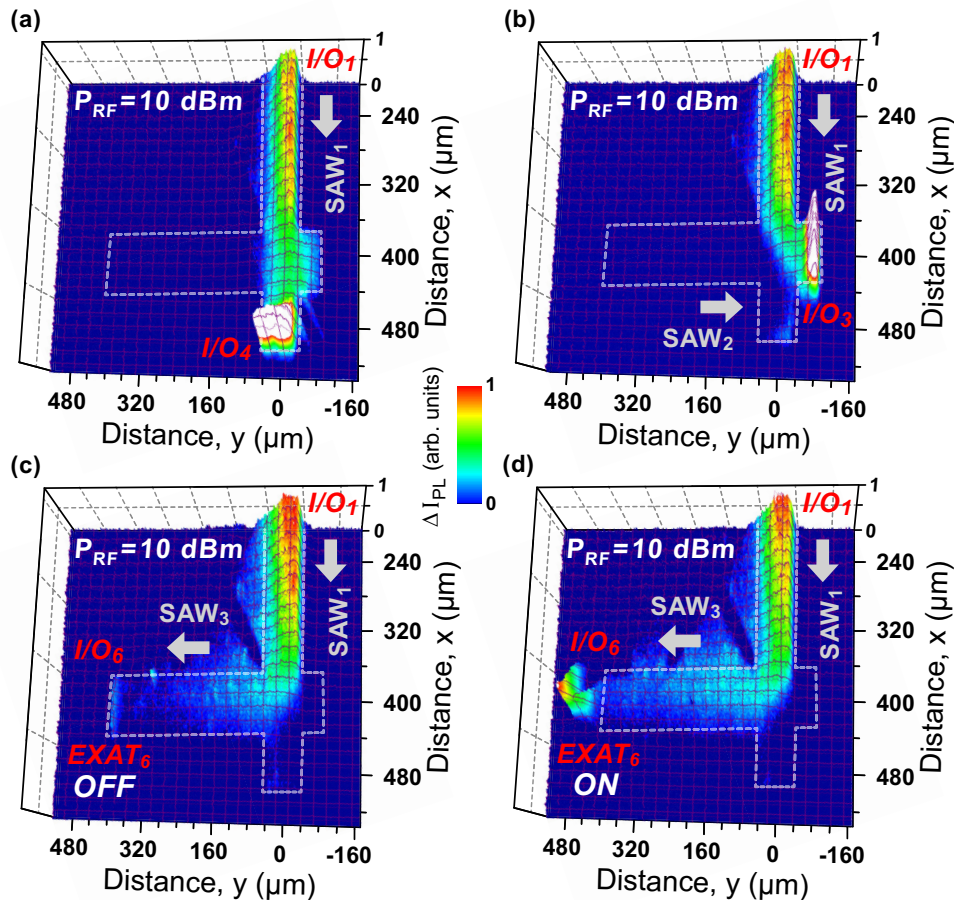


FIG. 4. (Color online) PL images of the acoustic IX transfer (a) along SAW_1 and between (b) SAW_1 and SAW_2 or (c) SAW_1 and SAW_3 . The output EXAT in (a)–(c) is in the OFF state. (c),(d) Control of IX flux by the gate electrode of EXAT_6 . All SAW beams are generated by applying $P_{\text{RF}} = 10$ dBm to the IDTs. The vertical (horizontal) dotted rectangle marks the transport channel formed by SAW_1 (SAW_2 or SAW_3).

EXAT source area and the common drain region, where multiplexing takes place. In each I/O port, an input optical signal [represented by a laser incident on the source electrode of EXAT₁ in Fig. 3(a)] can be converted into IXs and stored in the EXAT source electrode. Alternatively, stored IXs can be reconverted to photons by selecting an appropriate source voltage to reduce the IX recombination lifetime [34]. The EXAT source can act, therefore, as a voltage-tunable location for photon-to-exciton interconversion as well as for IX storage.

The straightforward IX transfer between two facing I/O ports [e.g., ports 1 and 4 in Fig. 3(a)] is carried out by simply turning the corresponding SAW and EXAT (i.e., SAW₁ and EXAT₁) ON. The multiplexing function relies on the transfer of IXs between two orthogonal acoustic beams (e.g., from the vertical beam SAW₁ to the horizontal beam SAW₂ or SAW₃) at their intersection area [*I* in Fig. 3(a)]. In this area, a moving array of potential dots is created by the interference of the two SAW beams. We have previously shown that the moving piezoelectric dots can efficiently transport uncorrelated electron-hole pairs between orthogonal piezoelectric SAWs [35]. A similar concept using a moving array of strain dots is applied here to transfer IXs between two nonpiezoelectric SAWs. As seen in Fig. 3(b), the dots propagate with a velocity $\sqrt{2}v_{\text{SAW}}$ (v_{SAW} denotes the SAW phase velocity) along channels, forming an angle of 45° with respect to the propagation directions of the two interfering SAWs [35]. Due to their oblique propagation direction, the dots can capture the IXs from the input beam and transfer them to the other beam, as illustrated in the time-averaged PL simulation of Fig. 3(c). The oblique lines show the propagation path of moving dots: a detailed numerical analysis of the transfer process including videos is presented in the SM.

The multiplexing action is illustrated by the PL images of Fig. 4. Figure 4(a) shows the direct transfer of IXs by SAW₁ from I/O₁ to I/O₄, which terminates close to the gate of EXAT₄ (kept in the OFF state). The transfer of IXs from SAW₁ to either SAW₂ or SAW₃ is demonstrated in Figs. 4(b) and 4(c), respectively. When SAW₂ (SAW₃) is switched ON, IXs transported by SAW₁ to the intersection area are captured by the moving potential dots and transferred to SAW₂ (SAW₃). While the dot propagation paths are not spatially resolved in the experiment, their oblique propagation [cf. Fig. 3(c)] is clearly observed within the intersection areas of the SAW beams in Figs. 4(b) and 4(c). The few IXs remaining within SAW₁ lead to the weak recombination observed in the lower part of this beam. From the PL image in Fig. 4(b), we determined that more than 90% of the IXs are transferred from SAW₁ to SAW₂ and recombine near EXAT₃, thus demonstrating a high beam-to-beam transfer efficiency. These results demonstrate that IXs can be reversibly transferred from any input port to any output port by appropriately switching on, at most, three SAW beams. The overhead time for switching will be established by the bandwidth of the IDTs and by the length of the SAW channels.

The PL images of Figs. 4(a)–4(c) have been recorded with the EXATs at the output ports in the OFF state, thus leading to the recombination of the transported IXs close to their gate electrodes. The combined action of long-range IX transport

with electrostatic EXAT switching is exemplified in Fig. 4(d). The image was recorded under the same conditions as Fig. 4(c), except that EXAT₆ was turned ON by changing its gate bias. Under these conditions, the IXs are transported to the transistor source area. Flow control by the EXAT gate electrodes, which can isolate the sources from the common drain, becomes particularly important for the electric control of IX storage and recombination using the source bias.

IV. DISCUSSIONS AND CONCLUSIONS

The results of the previous section show that IXs can be transported over long distances by SAWs. During transport, the IXs are kept within well-defined packets moving at a velocity close to the SAW velocity. As a result, IX transport can be easily synchronized with the pulse rate of an incoming photon beam by appropriately selecting the SAW frequency. The total transport distance between the input and output ports in Fig. 4(d) approaches 1000 μm, thus yielding IX lifetimes exceeding 380 ns. These transport distances, which are a factor of at least three larger than in previous reports, are limited by the length of the transport channel rather than by the acoustic transport efficiency (see Sec. III A). In fact, IX lifetime can be increased by at least another order of magnitude, thus allowing much longer transport lengths with minimal signal loss and distortion, which is essential for the scalability of exciton-based circuitry.

Another interesting feature of the SAW-induced transport is that the IXs remain trapped within the 50-μm-wide beams [outlined by vertical dotted rectangle in Fig. 4(a)]. The fabrication of the transport channels does not require lateral electrode structuring or the introduction of lateral interfaces, which can deteriorate the materials properties. Moreover, the EXAM concept is extensive to other systems and can be applied to interconnect an arbitrary number *N* of remote communication ports. In particular, if ℓ_p denotes separation between two adjacent ports, the lateral dimension of the two-dimensional EXAM arrangement of Fig. 3(a) will be given approximately by $N\ell_p/4$. The maximum acoustic transport distance d_{max} required to connect two ports in an EXAM with *N* ports will be approximately twice as large. The maximum transport distance (as well as the maximum required IX lifetime and transfer times) increases linearly with *N*. If additional ports (as well as isolating EXATs) are included in each of the channel sections in-between the intersection areas (“*I*” in Fig. 3), then d_{max} will become proportional to \sqrt{N} , thus making it easier to scale up the number of ports. Also, by decreasing the overlap length of the IDT fingers, the width of the SAW beams, and hence of the transport channels, can be further reduced. For a given length, the minimum channel width will be ultimately determined by SAW diffraction. The latter can be minimized by reducing λ_{SAW} or by shaping the SAW beams using focusing IDTs. All of these features make the acoustic transport a very attractive technique to interconnect remote exciton systems.

In conclusion, the integrated exciton device presented in this work delivers a proof of concept for a scalable optoelectronic circuit capable of performing multiple electronic operations

using IXs as the operation medium. The EXAM is a building block, which can be easily integrated with other devices for on-chip optoelectronic applications. Finally, the long-range IX transport by moving acoustic potentials can provide a versatile framework for the manipulation and coupling of other exciton phases, including IXs or exciton-polariton condensates.

ACKNOWLEDGMENTS

The authors thank M. Ramsteiner for scientific discussions and S. Rauwerdink and W. Seidel for technical support in sample processing. We gratefully acknowledge financial support by DFG Project No. SA 598/9.

-
- [1] R. J. Warburton, *Nat. Phys.* **4**, 676 (2008).
- [2] M. Baldo and V. Stojanović, *Nat. Photon.* **3**, 558 (2009).
- [3] K. Cohen, R. Rapaport, and P. V. Santos, *Phys. Rev. Lett.* **106**, 126402 (2011).
- [4] J. Kasprzak, M. Richard, S. Kundermann, A. Baas, P. Jeambrun, J. M. J. Keeling, F. M. Marchetti, M. H. Szymańska, R. André, J. L. Staehli, V. Savona, P. B. Littlewood, B. Deveaud, and L. S. Dang, *Nature (London)* **443**, 409 (2006).
- [5] R. Balili, V. Hartwell, D. Snoke, L. Pfeiffer, and K. West, *Science* **316**, 1007 (2007).
- [6] L. V. Butov, A. L. Ivanov, A. Imamoglu, P. B. Littlewood, A. A. Shashkin, V. T. Dolgoplov, K. L. Campman, and A. C. Gossard, *Phys. Rev. Lett.* **86**, 5608 (2001).
- [7] A. A. High, J. R. Leonard, A. T. Hammack, M. M. Fogler, L. V. Butov, A. V. Kavokin, K. L. Campman, and A. C. Gossard, *Nature (London)* **483**, 584 (2012).
- [8] G. J. Schinner, J. Repp, E. Schubert, A. K. Rai, D. Reuter, A. D. Wieck, A. O. Govorov, A. W. Holleitner, and J. P. Kotthaus, *Phys. Rev. Lett.* **110**, 127403 (2013).
- [9] A. T. Hammack, M. Griswold, L. V. Butov, L. E. Smallwood, A. L. Ivanov, and A. C. Gossard, *Phys. Rev. Lett.* **96**, 227402 (2006).
- [10] K. Kowalik-Seidl, X. P. Vögele, F. Seilmeier, D. Schuh, W. Wegscheider, A. W. Holleitner, and J. P. Kotthaus, *Phys. Rev. B* **83**, 081307(R) (2011).
- [11] A. Gärtner, L. Pechtel, D. Schuh, A. W. Holleitner, and J. P. Kotthaus, *Phys. Rev. B* **76**, 085304 (2007).
- [12] R. Rapaport, G. Chen, S. Simon, O. Mitrofanov, L. Pfeiffer, and P. M. Platzman, *Phys. Rev. B* **72**, 075428 (2005).
- [13] Z. Vörös, D. W. Snoke, L. Pfeiffer, and K. West, *Phys. Rev. Lett.* **97**, 016803 (2006).
- [14] D. A. B. Miller, D. S. Chemla, T. C. Damen, A. C. Gossard, W. Wiegmann, T. H. Wood, and C. A. Burrus, *Phys. Rev. B* **32**, 1043 (1985).
- [15] A. A. High, A. T. Hammack, L. V. Butov, M. Hanson, and A. C. Gossard, *Opt. Lett.* **32**, 2466 (2007).
- [16] A. A. High, E. E. Novitskaya, L. V. Butov, M. Hanson, and A. C. Gossard, *Science* **321**, 229 (2008).
- [17] G. Grosso, J. Graves, A. T. Hammack, A. A. High, L. V. Butov, M. Hanson, and A. C. Gossard, *Nat. Photon.* **3**, 577 (2009).
- [18] Z. Vörös, R. Balili, D. W. Snoke, L. Pfeiffer, and K. West, *Phys. Rev. Lett.* **94**, 226401 (2005).
- [19] A. Gärtner, A. W. Holleitner, J. P. Kotthaus, and D. Schuh, *Appl. Phys. Lett.* **89**, 052108 (2006).
- [20] A. G. Winbow, J. R. Leonard, M. Remeika, Y. Y. Kuznetsova, A. A. High, A. T. Hammack, L. V. Butov, J. Wilkes, A. A. Guenther, A. L. Ivanov, M. Hanson, and A. C. Gossard, *Phys. Rev. Lett.* **106**, 196806 (2011).
- [21] J. Rudolph, R. Hey, and P. V. Santos, *Phys. Rev. Lett.* **99**, 047602 (2007).
- [22] C. Rocke, S. Zimmermann, A. Wixforth, J. P. Kotthaus, G. Böhm, and G. Weimann, *Phys. Rev. Lett.* **78**, 4099 (1997).
- [23] J. A. H. Stotz, R. Hey, P. V. Santos, and K. H. Ploog, *Nat. Mater.* **4**, 585 (2005).
- [24] O. D. D. Couto, Jr., F. Iikawa, J. Rudolph, R. Hey, and P. V. Santos, *Phys. Rev. Lett.* **98**, 036603 (2007).
- [25] H. Sanada, Y. Kunihashi, H. Gotoh, K. Onomitsu, M. Kohda, J. Nitta, P. V. Santos, and T. Sogawa, *Nat. Phys.* **9**, 280 (2013).
- [26] O. D. D. Couto, Jr., S. Lazić, F. Iikawa, J. A. H. Stotz, U. Jahn, R. Hey, and P. V. Santos, *Nat. Photon.* **3**, 645 (2009).
- [27] E. A. Cerda-Méndez, D. N. Krizhanovskii, M. Wouters, R. Bradley, K. Biermann, K. Guda, R. Hey, P. V. Santos, D. Sarkar, and M. S. Skolnick, *Phys. Rev. Lett.* **105**, 116402 (2010).
- [28] M. M. de Lima, Jr. and P. V. Santos, *Rep. Prog. Phys.* **68**, 1639 (2005).
- [29] R. Rapaport, G. Chen, D. Snoke, S. H. Simon, L. Pfeiffer, K. West, Y. Liu, and S. Denev, *Phys. Rev. Lett.* **92**, 117405 (2004).
- [30] L. V. Butov, A. C. Gossard, and D. S. Chemla, *Nature (London)* **418**, 751 (2002).
- [31] A. Violante, K. Cohen, S. Lazić, R. Hey, R. Rapaport, and P. V. Santos (submitted).
- [32] We note that the IXs can also flow across an EXOT with the same source and drain bias if there is a density gradient or by a gradient in interaction energies between these two electrodes. These driving forces, however, cannot transfer all IXs in the source to the drain since they vanish as soon as a uniform concentration over the transistor channel (including the source and drain regions) is reached. They are, therefore, not appropriate for the transport of excitons as well-defined packets.
- [33] See Supplemental Material at <http://link.aps.org/supplemental/10.1103/PhysRevB.89.085313> for details of the model and additional simulation results.
- [34] A. G. Winbow, A. T. Hammack, L. V. Butov, and A. C. Gossard, *Nano Lett.* **7**, 1349 (2007).
- [35] F. Alsina, J. A. H. Stotz, R. Hey, and P. V. Santos, *Solid State Commun.* **129**, 453 (2003).